Distributed Brillouin fiber sensor for detecting pipeline buckling in an energy pipe under internal pressure

Lufan Zou, Xiaoyi Bao, Fabien Ravet, and Liang Chen

A distributed Brillouin fiber sensor has been employed to detect localized pipe-wall buckling in an energy pipe by measuring the longitudinal and hoop strain distributions along the outer surface of the pipe for the first time. The locations of the localized pipe-wall buckling are found and distinguished using their corresponding strain–load data. The formation of the buckling process for the compression and tension characters is studied in the longitudinal and hoop directions. For the pipe with internal pressure, concentric load, and bending load, a localized pipe-wall buckling takes place away from the middle of the pipe on the compressive side and a strain peak with an overall buckling occurs on the tensile side according to the longitudinal strain distributions along the pipe. Different strains on two neutral lines are also observed in the hoop strain distribution, which should be caused by the pipe weld joint.

OCIS codes: 060.2370, 290.5830, 290.0290, 060.2310.

1. Introduction

Pipelines provide one of the safest and most reliable means for transportation of liquids and gases. In the past few decades, the operating temperatures and pressures for oil and gas pipelines have dramatically increased. This change, combined with a trend toward using pipes of larger diameter, has increased the propensity for such pipelines to buckle in accordance with the greater axial loads.[1] If the pipeline is not free to expand but is restrained by friction, the pipe will be subjected to an axial compressive load. If the force exerted by the pipe on the soil cover exceeds the restraint created by the submerged weight of the pipe, its bending stiffness, and the soil cover, the pipe will tend to move, and considerable displacements may occur. Pipeline movement redistributes the axial force along the pipe, which results in increasing tension in some locations and compression in others. It can also raise the pipeline curvature, which induces the tensile strain in half of the pipe cross section and the compressive strain in the other half. The excessive tensile strain can lead to pipeline rupture, particularly at girth welds. The large compressive strain may cause buckling, usually accompanied by the formation of wrinkles that can rupture due to material fatigue or severe yielding. For the above reasons it is important to monitor the pipeline buckling before pipeline rupture happens. There is a desperate need for a real-time structural health monitoring (SHM) system that can intelligently monitor the integrity of underground pipelines.

Pipeline integrity and disturbance are generally not monitored due to the lack of reliable and durable techniques.[2] One of the major difficulties of monitoring pipelines stems from the fact that the pipelines can be buried hundreds of kilometers underground. Conventional conductive sensors have difficulties surviving their surrounding environments and have electrical noise problems. Furthermore, numerous such point-sensing devices are required to adequately monitor the health of long pipelines at a substantial cost. Since the buckling locations in a structure are not known *a priori,* conventional point sensors are not effective in buckling sensing. Fortunately, with the advent of optical fiber technology utilizing low-cost optical fiber communication cables, distributed SHM can be realized for pipelines.

Recently we reported the results using a distributed Brillouin fiber sensor (DBFS) to detect pre-embedded inner wall cutouts in an internally pressurized end-capped steel pipe.[3] To simulate the structural degradation caused by corrosion in pipes, rectangular indentations were entrenched within the inner wall of

The authors are with the Fiber Optics Laboratory, Department of Physics, University of Ottawa, 150 Louis Pasteur, Ottawa K1N 6N5, Ontario, Canada. L. Zou's e-mail address is lzou@uottawa.ca.

Received 26 July 2005; accepted 4 December 2005; posted 21 December 2005 (Doc. ID 63741).

0003-6935/06/143372-06$15.00/0

a steel pipe. Those pre-embedded defects comprising 50% and 60% of the inner wall thickness have been successfully discriminated using the corresponding strain measurements in the axial and hoop directions along the pipe. In this work, we conduct localized pipe-wall buckling monitoring in a piece of energy pipe that is 2667 mm (105 in.) in length and 762 mm (30 in.) in diameter by a coherent probe–pump-based Brillouin optical fiber sensor[4] with 15 cm spatial resolution. The distributed information at every 5 cm along the pipe is clearly shown in the corresponding strain measurements. Different locations along the pipe display different values of Brillouin frequency shift corresponding to different strains. The strain measurements taken by the DBFS match the strain readings collected by strain gauges where they were installed.

2. Experimental Procedures

A. Preparation of Localized Pipe-Wall Buckling Test

The test pipe is a piece of a natural gas transiting steel pipe that is 2667 cm (105 in.) in length and 762 mm (30 in.) in diameter, as shown in Fig. 1. The material specifications of the pipe are listed in Table 1. The pipe was sealed on both ends. To simulate a real situation of natural gas transit, the pipe was filled with water and the internal pressure was kept at 18.4 MPa (2669 psi) during the pipe-wall buckling test. The concentric and bending loads were employed by a Universal Test System (UTS). The concentric load was used to balance internal pressure. The strain measurements were taken at every 334 kN (75 kips) when the bending load was changed from 0 until the localized pipe-wall buckling occurred. Longitudinal directions of 6 and 12 o'clock along the pipe were subjected to tension and compression, respectively. Strain gauges were distributed longitudinally along the directions of 6 o'clock (tensile side) and both 3 and 9 o'clock (neutral lines). Three strain gauges were installed longitudinally along the pipe on the compressive side, as shown in Fig. 2. The external profiles of the pipe on the compressive side were also monitored by a laser scanner. A clinometer was used to measure the rotation of the pipe on the tensile side.

Table 1. Material Specifications of the Steel Pipe

Poisson's Ratio	Young's Modulus (30×10^6 psi)	Length (105 in.)	Outer Diameter (30 in.)	Wall Thickness (0.543 in.)
0.3	200 GPa	2667 mm	762 mm	14 mm

B. Installation of Sensing Fibers

To prepare the pipe for fiber installation, sandpaper was used to remove irregularities and provide a smooth, uniform surface around its circumference. An acrylate buffered SMF-28 optical fiber was used for monitoring both the environmental temperature conditions and the strain distributions along the pipe. Ten sensing sections were mounted externally on the pipe to monitor the strain changes on the outer surface and were protected by a specially designed adhesive, as shown in Fig. 2. Each 2 m sensing fiber was symmetrically located in the central portion of the pipe with a 1 m loose fiber separating one sensing section from another. The longitudinal strain distribution along the pipe can be measured from each sensing section, and hoop strain distribution around the circumference of the pipe at any location of the pipe can be obtained from these ten sensing sections. The environment temperature was kept constant during strain measurements.

C. Distributed Brillouin Fiber Sensor

The DBFS with centimeter spatial resolution used to detect pipeline buckling has been reported previously.[4] The system is based on the interaction of a probe pulsed laser plus a dc component with a counterpropagating cw laser for DBFSs at a wavelength of 1320 nm. The probe beam is subjected to Brillouin amplification at the expense of the cw beam. The

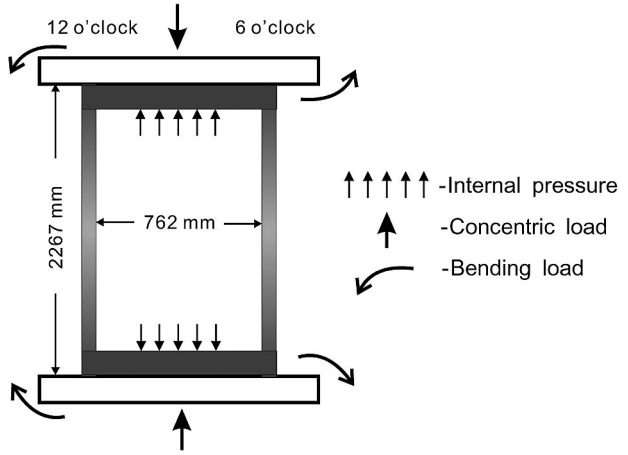

Fig. 1. Schematic diagram of an energy pipe used for the localized pipe-wall buckling detection and the UTS.

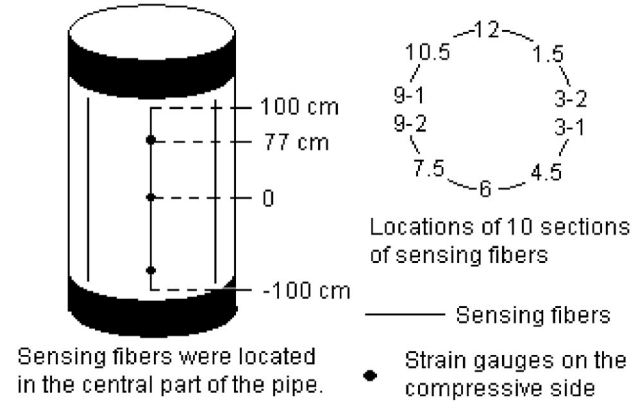

Fig. 2. Longitudinal layout of ten sensing sections with a 1 m loose fiber separation. Longitudinal distribution of strain can be measured from each section, and hoop strain distribution around the circumference of the pipe at any location of the pipe can be obtained from these ten sensing sections.

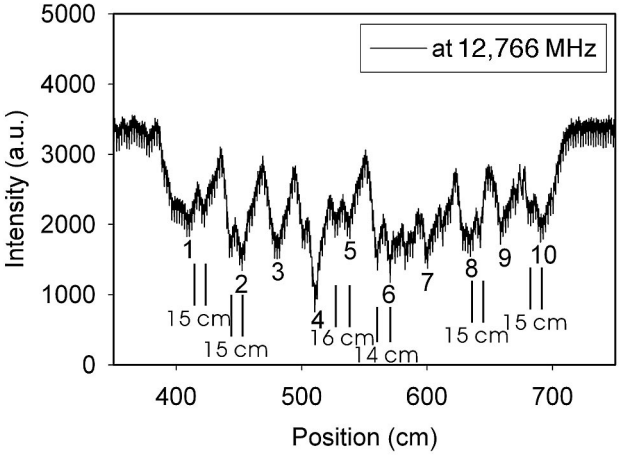

Fig. 3. Time-domain profile for a whole sensing fiber at 12,766 MHz before the bending loads are applied. Ten valleys correspond to ten sections of sensing fiber glued onto the pipe, and the fine structures in most valleys indicate 15 cm spatial resolution for our system.

resultant power drops in the cw beam are measured while the frequency difference between two lasers is scanned, giving the Brillouin loss spectrum of the sensing fiber. The Brillouin shift of the fiber is determined from the spectrum to calculate the strain of the sensing fiber. The measurement accuracy of strain is 15 $\mu\varepsilon$.[5] The spatial information is determined by the analysis of the cw signal in the time domain. A 1.5 ns duration was used in the measurements to give 15 cm spatial resolution. Brillouin spectrum measurements were acquired every 5 cm along a 29 m sensing fiber plus 60 m leading fiber every 20 min using 4000 averages.

3. Results and Discussion

Figure 3 displays the time-domain profile at ν_B = 12,766 MHz on a zero bending load, which clearly shows ten valleys corresponding to ten sections of sensing fiber glued onto the pipe. There are fine structures in most valleys because of nonuniform strains, which indicates 15 cm spatial resolution for our system. There was a 3354 kN (754 kips) load on the pipe before the bending loads were applied on the pipe, which causes the pipe-experienced compression, since the Brillouin frequency of SMF-28 optical fiber at 1319 nm should be 12,795 MHz at room temperature.

The strain distributions along the 12 o'clock section of the pipe on the bending load of 979 kN (220 kips) and 1335 kN (300 kips) are presented in Fig. 4. Obviously this section experienced more compression compared with that of a zero bending load. It shows clearly that our sensor system can offer continually distributed information of strain along the pipe. When the middle point of the pipe is chosen as the origin of an axis, for the bending load of 979 kN (220 kips) and 1335 kN (300 kips), the maximum compressive strains of -4391 and -7555 $\mu\varepsilon$ were observed at 40 cm. The ripples in the strain profiles

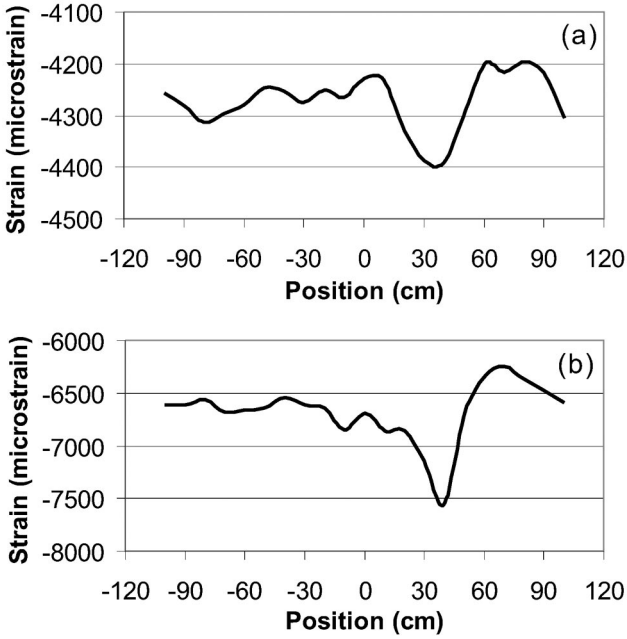

Fig. 4. Strain distributions along the 12 o'clock section of the pipe on the bending loads of (a) 979 kN (220 kips) and (b) 1335 kN (300 kips). The maximum compressive strains of -4391 and -7555 $\mu\varepsilon$ happened at 40 cm on the bending loads of 979 and 1335 kN, respectively.

represent pipe-wall deformations due to the compression of the pipe. With an increase in the bending loads, the valley of the strain profile becomes narrow and the compression maximum is increased as well. This predicts that a localized pipe-wall buckling will happen at this location.

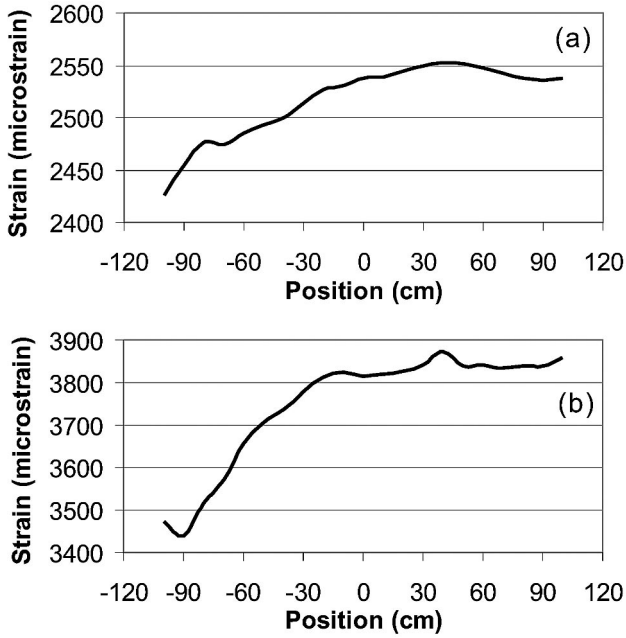

Fig. 5. Strain distributions along the 6 o'clock section of the pipe on the bending loads of (a) 979 kN (220 kips) and (b) 1335 kN (300 kips). The biggest tensile strain of 2553 and 3874 $\mu\varepsilon$ also occurred at 40 cm on the bending loads of 979 and 1335 kN, respectively.

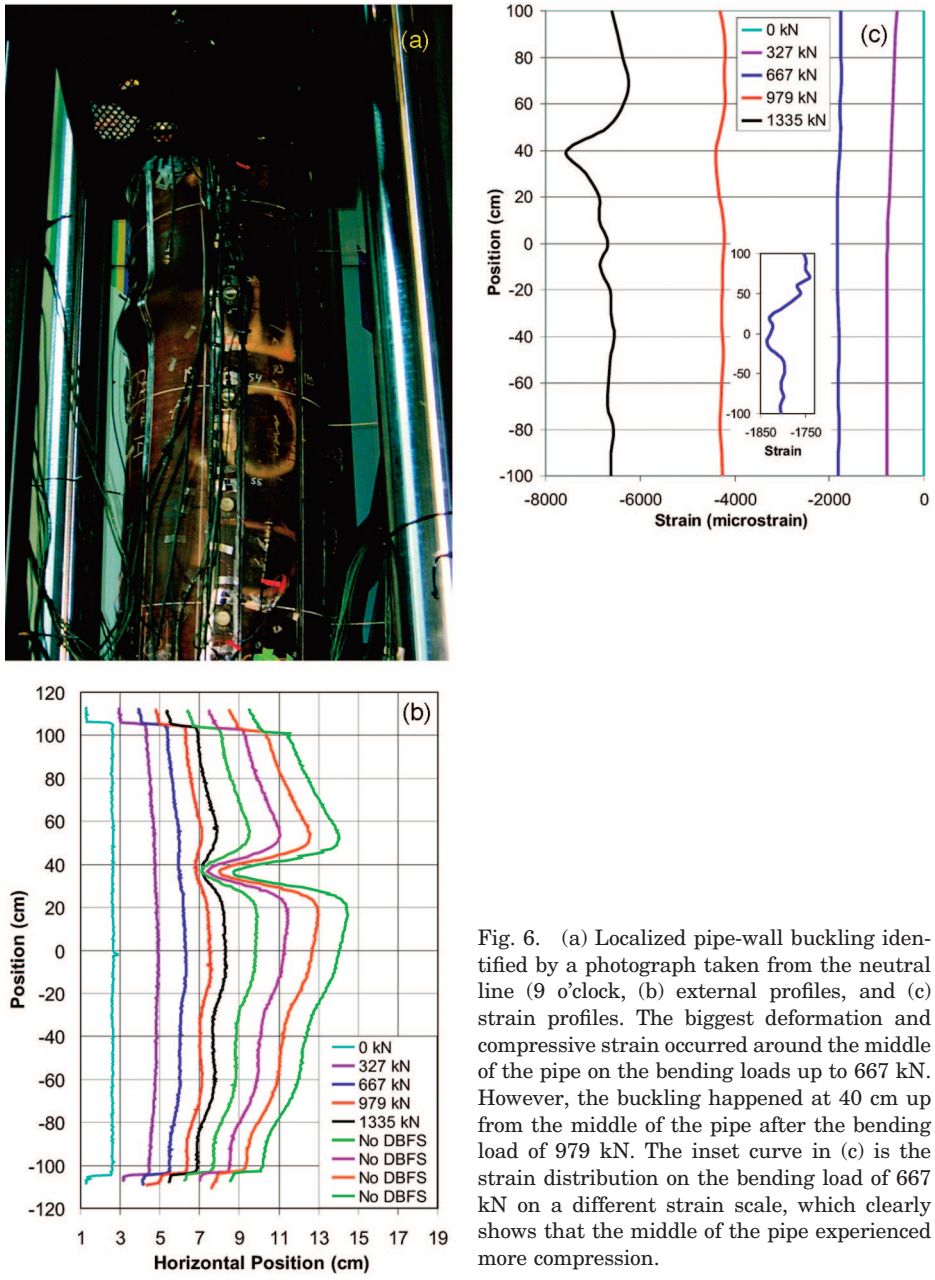

Fig. 6. (a) Localized pipe-wall buckling identified by a photograph taken from the neutral line (9 o'clock, (b) external profiles, and (c) strain profiles. The biggest deformation and compressive strain occurred around the middle of the pipe on the bending loads up to 667 kN. However, the buckling happened at 40 cm up from the middle of the pipe after the bending load of 979 kN. The inset curve in (c) is the strain distribution on the bending load of 667 kN on a different strain scale, which clearly shows that the middle of the pipe experienced more compression.

Figure 5 displays the strain distributions along the 6 o'clock section of the pipe on a bending load of 979 kN (220 kips) and 1335 kN (300 kips). The biggest tensile strain of 2553 and 3874 $\mu\varepsilon$ also occurred at 40 cm. Compared with the compressive side, the strain increases gradually along the longitudinal direction of the pipe to the location of 40 cm, then drops down gradually; also, there are no ripples in the strain profiles, which suggests no severe pipe-wall deformations on the tensile side. However, since the pipe at 40 cm experiences the highest tensile strain, it reminds us to pay more attention to the tensile side since some location on the tensile side may exceed the yielding point on certain loads.

When the bending loads were further increased after 1335 kN (300 kips), the Brillouin measurements were interrupted, since a sharp bending of the fiber induced by a localized pipe-wall buckling resulted in a broken sensing fiber on the compressive side. The test continued and the laser scanner was kept running. According to Figs. 4 and 5, we can identify that the localized pipe-wall buckling would happen around 40 cm, which is confirmed by the photograph shown in Fig. 6(a) that was taken after the test was finished and the profiles were collected by the laser scanner [Fig. 6(b)]. For comparison, the strain profiles measured by the DBFS are shown in Fig. 6(c). According to the profiles collected by the laser scanner, the buckling peak happened at 37 cm, whereas the strain peak occurred at 40 cm, [Fig. 6(c)]. The location uncertainty of the DBFS is limited by the digitizer's resolution: ± 5 cm. The location of buckling

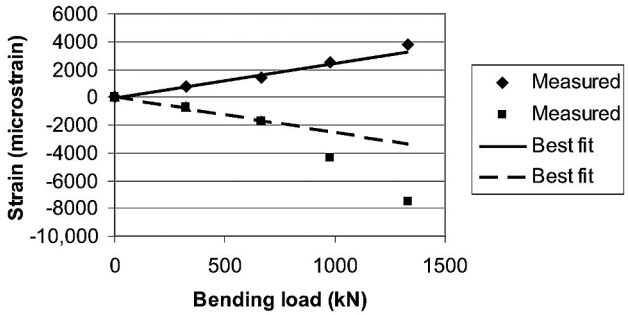

Fig. 7. Strain–load relation at the buckling location. The elastic coefficients are the same for both compression and tension. However, the buckling behavior on the tensile side is different from that on the compressive side, and the localized pipe-wall buckling would happen on the compressive side prior to on the tensile side.

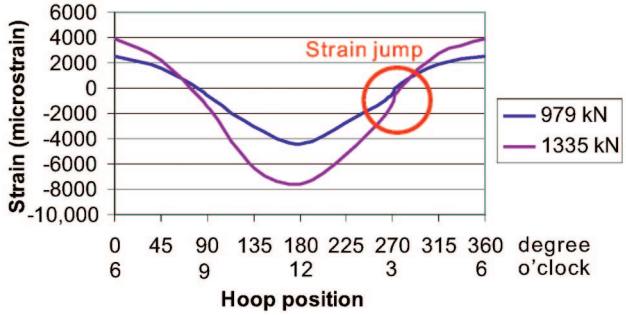

Fig. 8. Hoop strain distribution at the buckling location (40 cm up from the middle of the pipe). The maximum compression happened at around 180° (12 o'clock position), and when the bending load increased to 1335 kN (300 kips), the maximum compression then shifted to 11 o'clock. The strain changed smoothly at neutral section 9 o'clock from 83° to 97°, but there is a jump of strain at neutral section 3 o'clock from 260° to 277°, which should be caused by the pipe weld joint at 3 o'clock (270°).

identified by the DBFS is well matched with that collected by the laser scanner. It is well known that the laser scanner is not suitable for field monitoring because pipelines are buried underground and it cannot offer any strain information. Nevertheless, the DBFS can provide both strain and location information. To acquire the distributed strain information after a localized pipe-wall buckling occurs, we are investigating new types of high-strength optical fiber for SHM of pipeline.

According to the thin-shell theory,[6,7] the buckling should take place in the middle of the pipe on this kind of bending load, which was confirmed by another buckling test before this one under the same test conditions without internal pressure and concentric load (not shown here). To simulate gas transportation, the pipe in this test was filled with water for an internal pressure of 18.4 MPa (2669 psi). A concentric load was used to balance it, which was similar to the buckling test without internal pressure and concentric load. When the bending loads in this test were less than 667 kN (150 kips), the external profiles of the pipe and strain profiles show that the pipe experienced an overall buckling,[6] which looks as if a localized pipe-wall buckling should occur in the middle of the pipe [see Figs. 6(b) and 6(c)] when the bending load is increased. The inset curve in Fig. 6(c) is the strain distribution on the bending load of 667 kN on a different strain scale, which clearly shows that the middle of the pipe experienced more compression. However, the buckling finally took place at around 40 cm up from the middle of the pipe. The size and shape of the buckling in this test are totally different from those in the test without internal pressure and concentric load. Since the buckling location in this test was different from that predicted by the thin-shell theory and not known *a priori,* there were no strain gauges installed on the buckling locations, so no strain gauge readings were available for compression at the buckling point. There was a strain gauge installed at the middle point of the pipe. Its strain reading matched the compressive strains of -4330 and -6850 $\mu\varepsilon$ measured by the DBFS on the bending load of 979 kN (220 kips) and 1335 kN (300 kips), respectively. The strain ripple that resulted from the pipe-wall deformation on the bending load of 1335 kN (300 kips) is stronger than that on other bending loads. The more the bending load, the more the deformation of the pipe. Comparing the external profile with the strain profile on the bending load of 979 kN (220 kips), there are two peaks located at 39 and -29 cm in the external profile [see Fig. 5(b)]; thus it is not obvious that one can identify where the buckling will happen. However, the strain profile on the bending load of 979 kN (220 kips) clearly indicates that the buckling would occur at 40 cm since there is only one big strain peak [see Fig. 6(c) or Fig. 4(a)]. Obviously, it is more important for the DBFS to show signs of buckling on a lower bending load earlier than with the laser scanner. Therefore the DBFS is a powerful tool to monitor pipeline buckling before buckling happens.

Figure 7 illustrates the strain change with bending loads at the buckling locations of both compressive and tensile sides. The best-fit lines show the same elastic coefficients for both compression and tension because of the same material, which demonstrates the fact that our distributed sensor system can offer strain and location information accurately. For the same bending loads of 979 kN (220 kips), the buckling location on the tensile side was still in an elastic region; on the compressive side, however, it exceeded the yielding point, which means that the localized pipe-wall buckling would happen first on the compressive side. Along with the increase of the bending load up to 1335 kN (300 kips), the strain on the tensile side surpassed the yielding point; on the compressive side it exceeded the yielding point much farther than it did on the tensile side, so that the horizontal displacements of the pipe on the tensile side should not be the same as that on the compressive side in this test. In fact, overall buckling only happened on the tensile side, as seen in the photograph taken from the neutral line 9 o'clock [Fig. 6(a)]. Therefore the buckling behavior on the tensile side is different from

Table 2. Strains around Neutral Sections

Bending Load	Location: Neutral Line 9 o'clock 83° (9–2 o'clock)	Location: Neutral Line 9 o'clock 97° (9–1 o'clock)	Location: Neutral Line 3 o'clock 263° (3–2 o'clock)	Location: Neutral Line 3 o'clock 277° (3–1 o'clock)
979 kN (220 kips)	−135 με	−905 με	−961 με	340 με
1335 kN (300 kips)	−704 με	−2139 με	−2085 με	−39 με

that on the compressive side when the pipe experiences internal pressure and loads.

Since the pipeline length can be hundreds of kilometers, the measurement of hoop strain is inapplicable for SHM of pipeline. But if several longitudinal sensing fibers are installed around the circumference of the pipeline, the hoop strain at any location along the pipeline can be acquired. For example, in this buckling test we installed ten sensing sections longitudinally along the pipe for every 45° except for the 3 and 9 o'clock positions where there were two sensing sections in each position; we can also obtain hoop strain distributions around the circumference of the pipe at any location of the pipe. Typical hoop strain distributions at the buckling location (40 cm up from the middle of the pipe) are displayed in Fig. 8. The maximum compression happened at around 180° (12 o'clock position) and when the bending load increased to 1335 kN (300 kips); the maximum compression then shifted to 11 o'clock. For this test setup, 3 o'clock (270°) and 9 o'clock (90°) should be neutral lines. From Table 2, however, it can be found that the neutral line 9 o'clock (90°) experienced compression since both sides of 9 o'clock (90°) had compressive strain. The neutral line 3 o'clock (270°) might experience less compression than the neutral line 9 o'clock (90°) since one side (263°) of 3 o'clock is tension and the other side (277°) is compression on the bending load of 979 kN (220 kips); however, both sides experienced compression when the bending load increased to 1335 kN (300 kips). Because both 9–1 o'clock (97°) and 3–2 o'clock (263°) are located on same compressive side near their respective neutral sections, they have the same compressive strain (see Table 2). However, 9–2 o'clock (83°) and 3–1 o'clock (277°) show different strains, even though they are located on the same tensile side near their respective neutral sections. As shown in Fig. 8, the strain changed smoothly at neutral section 9 o'clock from 83° to 97°, but with a strain jump at neutral section 3 o'clock from 260° to 277°. These differences should be caused by the pipe weld joints at 3 o'clock (270°).

4. Conclusion

We have demonstrated the capability of a DBFS to detect localized pipe-wall buckling in an energy pipe that is 2667 mm (105 in.) in length and 762 mm (30 in.) in diameter by measuring the strain distributions along the outer surface of the pipe that experiences internal pressure and loads for the first time. The distributed information at every 5 cm along the pipe is clearly shown in the corresponding strain measurements. According to the longitudinal strain distributions along the pipe, for the pipe with internal pressure and concentric load, when the bending load was less than 667 kN (150 kips), the middle of the pipe experienced the maximum compression; however, when the bending loads increased, the buckling location changed, which has been identified successfully by our DBFS, even though it was not known *a priori.* For the test setup with bending load, tension and compression would happen on the opposite sides of the pipe. The elastic coefficients are the same for both compression and tension for the same material. However, the buckling behavior on the tensile side is different from that on the compressive side. The localized pipe-wall buckling would happen on the compressive side, and the strain peak with the overall buckling would occur on the tensile side. Different compressive and tensile strains, corresponding to different neutral lines, have also been observed in the hoop strain distributions. This demonstrates the ability of our system to differentiate the pipe weld joints from the rest of the pipe, even though it is on the neutral line on the bending loads. Our results show that the DBFS offers a great potential as a nervous system for infrastructure elements that allow high-performance, cost-effective health and damage assessment systems to be achieved.

The authors thank Joe Zhou and Keith Adams of TransCanada Pipelines Limited in Calgary, Alberta, Canada, for providing the pipe and associated help, and Tom E. Zimmerman of C-FER Technologies in Edmonton, Alberta, Canada, for providing the UTS and associated help.

References

1. D. J. White, A. J. Barefoot, and M. D. Bolton, "Centrifuge modeling of upheaval buckling in sand," Int. J. Phys. Model. Geotech. **2,** 19–28 (2001).
2. E. Tapanes, "Fibre optic sensing solutions for real-time pipeline integrity monitoring," presented at the Australian Pipeline Industry Association National Convention, Brisbane, Australia, 27–30 October 2001, http://www.iceweb.com.au/Newtech/FFT_Pipeline_Integrity_Paper.pdf.
3. L. Zou, G. A. Ferrier, S. Afshar V., Q. Yu, L. Chen, and X. Bao, "Distributed Brillouin scattering sensor for discrimination of wall-thinning defects in steel pipe under internal pressure," Appl. Opt. **43,** 1583–1588 (2004).
4. L. Zou, X. Bao, Y. Wan, and L. Chen, "Coherent probe-pump-based Brillouin sensor for centimeter-crack detection," Opt. Lett. **30,** 370–372 (2005).
5. L. Zou, X. Bao, S. Afshar V., and L. Chen, "Dependence of the Brillouin frequency shift on strain and temperature in a photonic crystal fiber," Opt. Lett. **29,** 1485–1487 (2004).
6. N. W. Murray, *Introduction to the Theory of Thin-Walled Structures* (Oxford U. Press, 1984).
7. P. E. Tovstik and A. L. Smirnov, *Asymptotic Methods in the Buckling Theory of Elastic Shells* (World Scientific, 2001).